

RGBD2lux: Dense light intensity estimation with an RGBD sensor

Theodore Tsismelis^{1,2,3}, Irtiza Hasan^{3,1}, Marco Cristani^{2,3}, Alessio Del Bue^{3,†}, Fabio Galasso^{1,†}
 Corporate Innovation OSRAM GmbH¹, Istituto Italiano di Tecnologia (IIT)², University of Verona (UNIVR)³

t.tsismelis@osram.com, irtiza.hasan@univr.it

Abstract

Lighting design and modelling or industrial applications like luminaire planning and commissioning rely heavily on physically correct simulations. The current typical approaches are based on CAD modeling simulations and offline rendering, with long processing times and therefore inflexible workflows. Thus, in this paper we propose a computer vision based system to measure lighting with just a single RGBD camera. The proposed method uses both depth data and images from the sensor to provide a dense measure of light intensity in the field of view of the camera. We evaluate our system on novel ground truth'ed data and compare it to state-of-the-art commercial light-planning software. Our system provides remarkable performance, while being completely automated, given that the CAD model is extracted from the depth and the albedo estimated with the support of RGB images. To the best of our knowledge, this is the first automatic framework for the estimation of lighting in general indoor scenarios from RGBD input.

1. Introduction

Most lighting systems around us are the result of a careful design by lighting professionals and architects. This is the case of offices, whereby the level of light on each desk is regulated by ISO standards, of retail shops (according to specific marketing strategies), and of industrial sites, whereby lighting means safety for the human operators. In recent years, most sectors have changed to more agile strategies, e.g. reconfiguring the position of office desks in due course according to the need, which is not reflected any more in the designed lighting system.

The industrial-driven process of designing and creating lighting systems relies heavily on computer graphic based simulations. These approaches have been given an increased scientific attention [26, 35, 36] with modern systems where the light design process can be carried out in a completely interactive way using novel methods from the

field of visual computing [4, 24].

Besides such improvements, this process requires a strong manual intervention, using tools that are essentially custom-build computer graphics and computer-aided design (CAD) software [1, 2, 3]. All methods provide dense light intensity measurements through simulation, but they are based on simplified CAD models of a scene and they require to manually assign the reflectance properties of each structure and object present in the environment.

On the other hand, the only alternative for measuring light is hardware-based and it relies on the use of luxmeters, a device that normally provide a point-to-point measurements (i.e. sparse) of light intensity. This means that the operator needs to repeat the measurements in several positions of the environment, swaying for angular and spatial completeness and as a consequence being a very time and cost-expensive procedure.

In this paper, we propose an efficient solution to light measurement which uses commodity hardware (an RGBD sensor) and it provides dense pixel-level measurements of the light intensity in real environments. We leverage best features from the CAD-based simulation approaches, such as dense lighting measurements, but we bypass the user input of the CAD and reflectance model by means of the RGB (for the albedo) and depth (for the geometry) imaging. This results in an automatic procedure, which reaches the accuracy required by lighting designers.

Figure 1 shows a graphical description of our system (RGBD2lux). In general, the RGBD camera is installed to provide a top-view of the indoor environment¹. Given the depth information, we extract a partial mesh in the field of view of the camera. At the same time, for each patch of the mesh we estimate the reflectance as a scalar value (albedo) from multiple images with different light sources activated. Finally, the 3D mesh and reflectance are then used in a radiosity model that provides us with the overall estimation of the scene illuminance. The proposed system is then evaluated against ground truth readings from a set of luxmeters

[†]These two authors contribute equally to the work.

¹This is a practical solution since it provides the least occluded view of an indoor environment, however our method by design could work from any viewpoint.

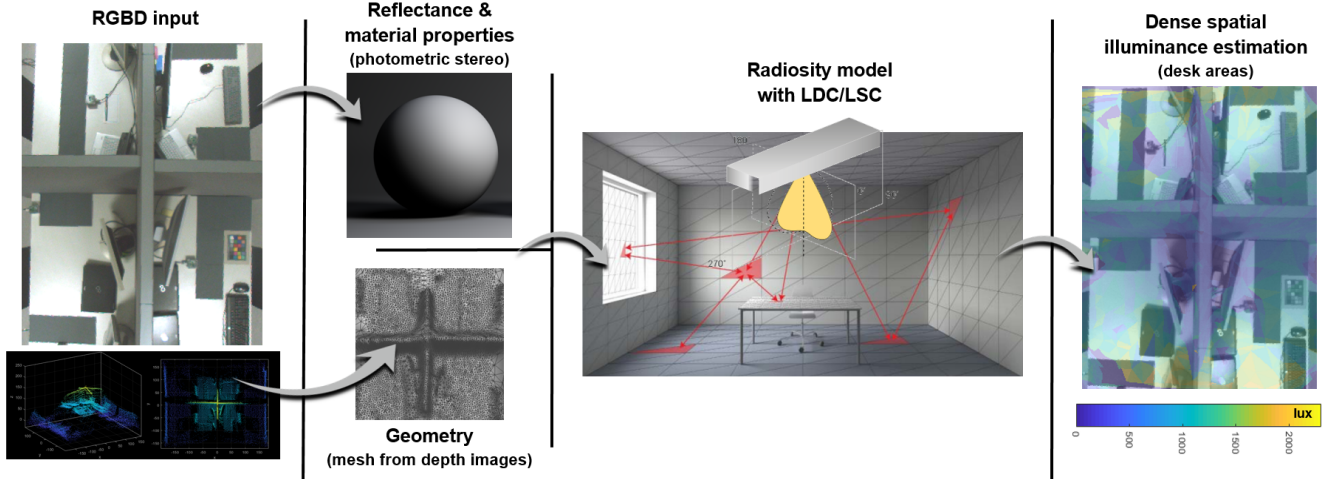


Figure 1. Pipeline of our system. We first acquire the RGBD input from the camera system (left), we then use the RGB image for extracting the albedo values of the surfaces based on a photometric stereo solution and the depth images for extracting the actual surfaces and the partial geometry of the scene (center). Both are then fed into our radiosity model using known light sources distribution curves. Lastly we measure the estimated illumination over the visible scene. See the estimated illumination over the desk areas (right).

showing its potential as a new system for dense light measurement.

The rest of the paper is organized as follows. Section 2 presents related work and the system introduced in this paper. Then Section 3 describes step by step the system for estimating light intensity from RGBD images. In Section 4 we introduce the benchmark and conduct experiments and ablation studies. Finally Section 5 concludes the paper.

2. Related Work

Measuring light is a problem that can be addressed by different fields. In the following we review three major topics in the literature related to light measurements.

Image processing. According to Cuttle *et al.* [14] the lighting profession and lighting evaluation procedures are moving from the conventional illuminance-based towards the luminance-based. That means to move from assessing light incident on planes (*e.g.* illuminance) towards the assessing light arriving at the eye (*i.e.* luminance). Given this change, the works in [8, 10, 17] take advantage of the emergence of camera-aided light measurement solutions. Hiscocks *et al.* [17] in his white paper provides an overall understanding of the luminance measuring procedure with a digital camera. Choo *et al.* [10] makes use of such a procedure for obtaining the luminance in a small simulated environment, structured from a carton box, a cheap web camera and a processing unit. On the other hand, Cai *et al.* [8] instead focused on to a more advanced solution by taking advantage of the high dynamic range (HDR) computational photography and its corresponding high quality equipment. However, all the previous mentioned solutions require a pre-calibration step of the camera sensor where pixel values are

mapped according to a known luminance source. However, the light amounts illuminating a surface simply are not reliably recoverable from a pixel-like array of radiance values, because they are the product of the irradiance, the surface reflectance, and complex interreflections between all surfaces in the 3D scene. Untangling them is very challenging in the general case as well explained in the pioneering works on “*inverse rendering*” by Ravi Ramamoorthi and Hanrahan [34], Steve Marschner [32], and others.

Computer graphics. Light modeling and understanding are also studied in computer graphics for the creation of photo-realistic renderings [18], [31]. The forward and inverse light transport theory physically simulates the path of transmitted light in a 3D environment and models the image as an integration process. This formalization requires the 3D environment structure, the material surfaces and many other physical properties [9, 23, 39]. To this end, many light models are proposed for retrieving and rendering scenes with as much as possible lifelike illumination. The most well known model is Radiosity [11, 15], popular for its simplicity and efficiency. Other more advanced and recent approaches are the instant radiosity [22] with its bouncing energy and the Virtual Point Lights (VPL), photon mapping [19] and progressive photon-tracing [16] with the idea of tracing photons from a light source through the scene and store their hits on diffuse surfaces in a so-called photon map.

Light design software. Relux [3], DIALux [1] and AGi32 [2] are commercial CAD-design modeling software products, and commonly used in the lighting design field, for measurement and evaluation of lighting solutions. The luminaire data is taken from photometric measurements provided by luminaire manufacturers, the material and photo-

metric properties are retrieved from online libraries while the geometrical structure needs to be known in advance. The light simulation process in all these software is based on the radiosity method, and different variants of it [5]. Recently HILITE and LiteMaker [4, 24], two prototypes with a new approach for lighting design, are currently being developed in an academic environment. They try to combine a physically based real time rendering with an interactive lighting simulation for complex architectural environments. The former uses a many-light global-illumination solution baked in light maps, including glossy material [27, 28], while the latter combines a multi-resolution image filtering technique with an interactive, progressive photon-tracing algorithm [16].

Our proposal. We bring together the best of image processing and light design software: we start from RGBD images and do not require user inputs; as in lighting design software, we target per-pixel exact lighting intensity estimates using a radiosity model that accounts for realistic environments. By contrast, computer graphics approaches pose emphasis on photorealistic appearances, caring more for shadows, reflections, liquids and smoke, rather than the actual lighting measure as we are interested in this application.

3. RGBD2lux approach

Here we describe the proposed indoor RGBD camera-aided light modeling system for real scenes. Our computational pipeline, as shown in Figure 1, first extracts a partial description of the indoor space geometry (*i.e.* a 3D mesh) and it computes a simple reflective model for every object in the scene (Sec. 3.1). Given these two outputs and knowing the position of the light sources, it is possible (Sec. 3.2) to estimate illuminance using the radiosity model that is enriched (Sec. 3.3) to account for real luminaries responses and specific light sensitivity curves.

3.1. Camera-aided 3D and reflectance modelling

Most simulated environments used for light intensity estimation need the a priori information of the CAD model and the material properties of the objects in the room. This is often hard to obtain in every lighting setup scenario and, when the CAD model is available, it is common to contain structural inaccuracies of the environment. To this end, we use a depth sensor for retrieving the coherent information of the indoor environment 3D structure without using a CAD model. The main goal here is to reconstruct the surface from the point cloud, represent it as a pair of vertices and faces and associate at each face a scalar albedo value.

The main issues to deal with is that depth sensors provide a sparse and noisier point cloud from which it is difficult to obtain a complete CAD like representation. Thus, given an exemplar point cloud from the RGBD sensor, we first apply

a denoising procedure to remove any outlier points, we then apply a mesh reconstruction solution based on Poisson surface reconstruction [21] approach and finally we post process the mesh with a Laplacian smoothing filter.

Using instead the images from the RGBD sensor, we record a time lapse video of the scene undergoing light variations given by the activation of the different light sources (*i.e.* luminaries) in the room. Then we select a subset of images with the LIT method [37] for which a single light source only is active. We use such images to estimate the pixel-wise albedo ρ using a first-order spherical harmonics model [6] with surface normals obtained from the previous surface reconstruction step. Even by using an approximated model, we compute a scalar reflectance values for each image pixel that experimentally provides satisfactory performance. Then these values are mapped to the surface faces as the mean value of the pixels, of the albedo map image, falling within the area of each triangle.

Given the partial 3D surface of the indoor environment, the scalar reflectance we can now apply the radiosity model in order to estimate the illuminance at each surface patch.

3.2. Light modelling - Radiosity

The radiosity model [29, 12] represents the current state-of-art model in all commercial lighting simulation software in the lighting field (Relux [3], DIALux [1], AGi32 [2]). With more details, radiosity models the light arriving at each point within a 3D scene by considering both direct light sources and inter-reflections. Given our 3D mesh discretized into a set of n triangular faces, we aim to compute the radiosity r_i at each patch $i = 1 \dots n$. r_i is measured in $[W/m^2]$ and is given by the direct emission of the room active sources (*e.g.* the room luminaries) plus the inter-reflection given by the other patches. Regarding the information about the light source position in 3D and their luminous intensity, we consider it as known, since luminaries may hardly be moved after their installation. Thus, the patches corresponding to the light sources are assigned with an emitting intensity value equal to the luminous intensity of the luminaires.

Given the available information, we can write the expression for radiosity with linear equations as:

$$r_i = e_i + \rho_i \sum_{j=1}^{n-1} f_{ij} r_j \quad (1)$$

where i and j index the n patches, e_i is a scalar expressing the self-emittance of patch i ($e_i = 1$ for light source patches in the unit measure, 0 otherwise), ρ_i is the isotropic reflectivity of patch i and f_{ij} is the form factor between patch i and j .

Form factors encode two main aspects:

- **Visibility**, if two patches are visible one from each

other, *i.e.* this value is equal to zero if there is no line of sight between them;

- **Distance and orientation**, encoding how well two patches “see each other”, *i.e.* low values correspond to very far patches with an oblique line of sight, high values instead refers to close fronto-parallel patches.

They are further constrained to be strictly non-negative and satisfy the reciprocity relation $a_i f_{ij} = a_j f_{ji}$, where a is the area of each patch (note that the reciprocity relation is not symmetric unless the patches have the same size).

Eq. (1) can be expressed as a global model by stacking all the equations and thus obtaining a linear system $\mathbf{F} \mathbf{r} = \mathbf{e}$ such as:

$$\underbrace{\begin{bmatrix} 1 - \rho_1 f_{11} & -\rho_1 f_{12} & \cdots & -\rho_1 f_{1n} \\ -\rho_2 f_{21} & 1 - \rho_1 f_{22} & \cdots & -\rho_2 f_{2n} \\ \vdots & \vdots & \ddots & \vdots \\ -\rho_n f_{n1} & -\rho_n f_{n2} & \cdots & 1 - \rho_1 f_{nn} \end{bmatrix}}_{\mathbf{F}} \underbrace{\begin{pmatrix} r_1 \\ r_2 \\ \vdots \\ r_n \end{pmatrix}}_{\mathbf{r}} = \underbrace{\begin{pmatrix} e_1 \\ e_2 \\ \vdots \\ e_n \end{pmatrix}}_{\mathbf{e}} \quad (2)$$

where \mathbf{F} is a $n \times n$ square matrix describing the geometry of the whole room, the n -vector \mathbf{r} contains the associated radiosities at each patch and the self-emission \mathbf{e} contains non-zero values at patches corresponding to active light sources. Now, solving for \mathbf{r} requires the knowledge of geometry \mathbf{F} , object reflectance ρ_i and the luminous intensity of the light sources \mathbf{e} .

In order to compute the form factors, we uniformly sample rays within the unit disc (*i.e.* the orthogonal projection of the unit sphere), whereby each point on the unit disc defines the direction of a ray in the space. Following [30], we compute f_{ij} as the ratio:

$$f_{ij} = \frac{m_j}{m_i}, \quad (3)$$

where m_j stands for the number of rays emitted by patch i that reaches patch j , and m_i is the total number of rays emitted by facet i .

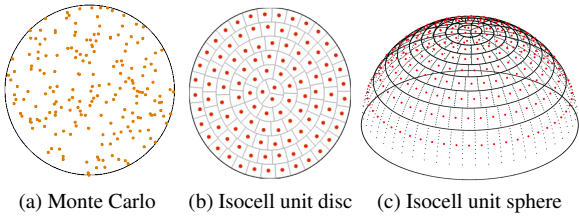


Figure 2. Illustration of the two different ray distribution methods.

As shown in Fig. 2, there are different methods to distribute the rays *e.g.* the Monte Carlo method [13], [20], *i.e.* the ray orientations are sampled randomly, see Fig. 2a. This method always converges but requires a great number of

rays to achieve a good precision, thus being computationally demanding. Instead we sample points in the unit disc (and therefore ray directions) by the approach of Masset *et al.* [33], [7], noted as “Isocell”, due to its higher precision within a fixed computation time. This is based on a uniform discretization of the ray orientations (*c.f.* Fig. 2b). In our implementation, given our patch discretization and room size, we found that 1,000 rays for each patch is a good compromise between accuracy and speed (*c.f.* Fig. 3c illustrates Isocell unit sphere rays, for a single patch on the office floor, within the CAD model). Thus, for computing the matrix f_{ij} we iterate through each patch and project the rays into the space from its center point and then we assign the corresponding form factor value according to the ratio described by Eq. (3).

Finally once we have populated the view factors matrix f_{ij} we need to ensure the reciprocity relation mentioned earlier. Here we adopt the iterative scheme of Van Leersum *et al.* [38] that can be considered as a refinement of the naive form factors rectification.

3.3. Customizing radiosity for real environments

The radiosity model in Eq. (2) has two limitations: it assumes point light sources and it disregards the light perception. We address both aspects in our model extension, by introducing the LDC (for considering any light source) and the LSC (to model the light observer / sensor perception).

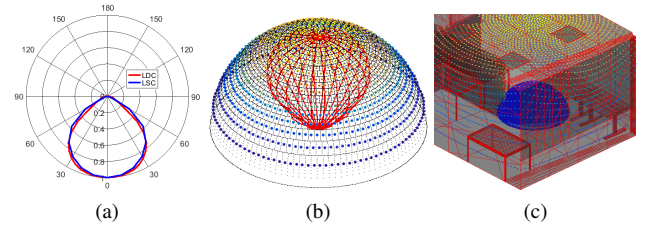


Figure 3. (a) Radial representation of LDC and LSC curves, illustrating how both quantities are attenuated (radius) with the growing light incident angle (radial angle); (b) weighted ray distribution of the Isocell unit sphere for LDC, heatmap-color-coded; (c) Isocell unit sphere (blue hemisphere) for a patch on the floor of the office CAD. The color-dots in (c) are taken from (b) but placed at the intersection of the cast ray with the other scene patches.

Light distribution curve (LDC). Let us recall Equations (1) and (2). The radiosity model uses a scalar variable e_i to set whether each patch is a light source ($e_i > 0$) or not ($e_i = 0$). The actual e_i value would relate to the radiant intensity or luminous flux of the light source, measured in lumens [cd/sr]. Since it uses scalar values, the Radiosity formulation of Section 3.2 assumes isotropic light sources, *i.e.* active patches radiate with the same intensity in all directions.

But isotropy is hardly the case for real light sources

which are normally represented by a radiation map, such as in Figure 3a (*red*). Their distribution is in general non-linear and encoded in a light distribution curve which provides the radiant intensity with respect to distance and angle from the emitting source (*i.e.* how much light is emitted in each direction). The LDC curves are obtained experimentally in lab environment conditions with the use of specific equipment, *i.e.* goniophotometer, and provided in datasheets by the luminaire manufacturer.

Thus, similarly to the existing solutions we include the LDC curve into the ray tracking procedure of our application and therefore we encode the non-linear radiation of light sources into the form factors f_{ij} . In more detail, we associate scalar values to each light source patch cast ray, which are proportional to the angle of emission, as illustrated in Figure 3b. These are then used to re-write Eq. (3) as a weighted mean. Since this procedure encodes the non-linear LDC into the form factors, our re-formulation of radiosity preserves the linearity of Eq. (2).

Note that, in this way, the non-linearity is embedded in the form factor computation process, which is already non-linear. This results therefore in a minimal impact on computation, since the system in Eq. (2) remains linear.

Light sensitivity curve (LSC). People perceive light differently, depending on their orientation with respect to it and depending on the distance from it. In a similar fashion, luxmeter sensors have different sensitivity to lighting, depending on the lighting angle and distance as well as to manufacturing characteristics. The LSC plot in Figure 3a (*blue*) illustrates the perception characteristic of the luxmeter which we adopt in order to meet the measuring requirements of the collected ground truth data. Note the strong similarities to LDC as in Figure 3a (*red*).

Therefore, we correct the sensor’s light perception by the LSC. Similarly to the LDC, we formulate the corresponding weighted Isocell unit sphere, as in Figure 3b, and integrate the weights into the form factor calculation by modifying the ray casting. In this way, we maintain the Radiosity linear formulation and alter the computation time minimally. It is worth mentioning here that interestingly enough this functionality is not applicable in any commercial light planning software available in the market.

3.4. Method resume

Algorithm 1 resumes the steps of the RGBD2lux approach necessary to estimate light intensity using a RGBD sensor and aligns it with the key elements of the radiosity light modeling.

Once the radiosity values are computed, they can be converted to illuminance considering the Lambertian assumption [25] and the fact that reflections are scattered isotropically and thus the illumination intensity is not a function of

Algorithm 1: RGBD2lux method.

- 1 From depth data compute a 3D mesh, see sec. 3.1 ;
 - 2 From a time-lapse video sequence, identify a subset of images with single light activations and run photometric stereo to find the albedo values ρ , see sec. 3.1 ;
 - 3 Compute the form-factors f_{ij} given the 3D mesh model, see sec. 3.2 ;
 - 4 For the 3D patches related to light sources apply the LDC computation of form factors, see sec. 3.3 ;
 - 5 For the 3D patches where perceived light is measured, apply the LSC computation of form factors, see sec. 3.3 ;
 - 6 Solve for the radiosity equation 2, see sec. 3.2 ;
-

the direction of the ray/beam:

$$L_{(x,y,\theta,\phi)} = L_{(x,y)} \neq f(\theta, \phi)$$

but instead will be constant for different sets of measuring equipment and directly proportional to the exitance intensity $E_{(x,y)}$ with a conversion factor of k :

$$E_{(x,y)} = L_{(x,y)} \cdot k = L_{(x,y)} \cdot \frac{\pi}{\rho}$$

where $E_{(x,y)}$ is the illuminance measured in lux and $L_{(x,y)}$ the radiance.

4. Experimental Evaluation

Experiments are organized as follows. Sec. 4.1 presents a novel dataset for light measurements. Sec. 4.2 shows quantitative results while Sec. 4.3 describes in more details the evaluation of our radiosity model against state of the art approaches. Finally, Sec. 4.4 reports real experiments with the RGBD data only.

4.1. Light measurement benchmark

To the best of our knowledge, there is currently no dataset for benchmarking light measurements with ground truth in real scenes. Thus, we define a new benchmark for light measurement in real world scenes. We select two different office rooms, namely room_1 and room_2, see Figure 4. As shown, we provide a detailed CAD design for the rooms representing the 3D ground truth. This includes an accurate labelling of the object textures and reflectivities for each surface facet in the CAD.

Both rooms have been equipped with a controlled lighting environment, since the position of eight luminaries is known (Fig 4b), as well as their type (Siteco Mira), meaning that the LDC curve is given by the manufacturer. Furthermore, to achieve even more accurate ground truth, we measured in lab conditions the overall luminous flux and tem-

perature of each luminaire being $7913lm$ and $4250k$ respectively, while the multiplicative parameter for the luminaire age² is assigned to value 1 since the installation is fairly new.

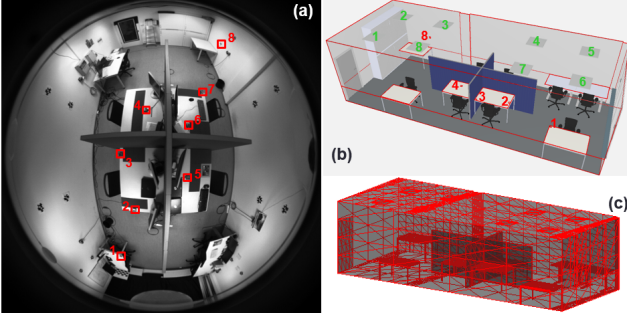


Figure 4. Room_1 full scene. (a) illustrate image as it looks from the camera, red bounding boxes are showing the location of luxmeters within the indoor space. Images (b) and (c) are detailed CAD design of the room showing the luminaire positioning and how the scene is scattered to individual patches respectively.

We provide for both rooms a number of sensory data. First, we set up in the ceiling of the rooms a RGBD calibrated and aligned sensory system which consists of an rgb camera with fish-eye lens with 180° FOV and a depth camera (Bluetechnix time-of-flight) with 90° FOV. However, in our experiments we consider only the part that is visible to both images after we have registered and undistorted them (as shown in Fig. 1, left).

The sensors are synchronized with luxmeters (also indicated in Fig. 4a and 4b), providing therefore the ground truth data for illumination intensity. The luxmeters however give localized (*i.e.* point-to-point) lux readings only, so we installed 8 of them in different areas so providing a reasonable sampling of the environment. We chose mainly locations over desk areas, since they are of major importance in the lighting field. For each luxmeter, we additionally report the type and their specific light sensitivity characteristic curve (LSC, see Fig. 3a), namely the sensor sensitivity across the incident light angles.

Thereafter, we evaluate 31 different luminaire activations (luminaires switched on or off) for each room, see Fig. 5 for a sample of images obtained from room_1. We target the use of rgb and depth input just for light measurement, the use of luxmeters as ground truth, and all other provided information for ablation studies.

4.2. Quantitative comparisons in Lux

Table 1 summarizes the overall performance of the commercial light modeling software Relux, compared to ours and both to the ground truth under all the different exper-

²The efficiency of every luminaire degrades over time.

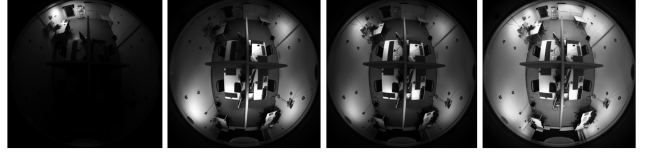


Figure 5. Illustration of 4 illumination variants within room_1. From the left, the images illustrate the illumination provided by 1, 3, 4 and all 8 luminaires switched on in the scene.

imental inputs. Beyond the proposed RGBD2lux, which does not require the CAD model and integrates the LDC and LSC curves, we additionally compare Relux to our own model using the CAD input provided (*i.e.* **Ours with CAD**). Results are reported for both room_1 and room_2.

Note that, when provided with the CAD model, our model outperforms Relux, thanks to the induced LDC and LSC distributions into the radiosity. In fact, against ground truth, **Ours CAD (LDC.LSC)** achieves an average luxmeter error (across all 1-8 luxmeters) of 36 Lux for room_1 and 70 Lux for room_2³. These errors are 9.2% and 3.7% better than Relux, for room_1 and room_2 respectively.

Our proposed RGBD2lux (modelling LDC and LSC but not requiring the CAD) is still comparable with the Relux (instead requiring the CAD). Here we only consider the luxmeters in the area visible from the depth-camera (**Avg (2-7)**), *i.e.* those for which RGBD2lux may compute a Lux value. For room_1 we achieve an error of 61 Lux, and for room_2 we achieve an error of 99 Lux. Thus, in this case the average lux error percentage is respectively worse than Relux by 4.6% for room_1, and by 8.1% for room_2.

It is of interest to note how the consideration of LSC provides a larger error reduction than LDC (rows 6 and 7 in the table), consistently across the two rooms. We interpret this as the way the form factors matrix is populated, *i.e.* based on the ratio between the rays arriving at a patch by the overall emitted rays, where there is a higher dependency on the emitted rays rather than the received rays, which would otherwise be equally strong from any angle.

4.3. Comparisons against Relux using CAD models

Here we analyze in more details our system against the commercial Relux software [3]. For comparability, since Relux requires the CAD model, we provide it also to ours. These experiments provide a sanity check (since Relux also uses radiosity), a detailed analysis on the contribution of LDC and LSC curves, and the effect of considering the visible scene just.

Figure 6 shows six box plots of the light measurement error (y-axis), as measured by each of the 8 installed luxme-

³The supplemental material describes which are the structural differences between the two rooms together with the reason why room_2 is more complex in terms of light modelling than room_1

| | Room 1 Error (in Lux) | | | | | | | | | | Room 2 Error (in Lux) | | | | | | | | | |
|--|--------------------------|-----|----|----|----|----|----|----|---------------|---------------|--------------------------|-----|----|-----|-----|-----|----|----|----------------|----------------|
| | Luxmeters | | | | | | | | Avg. (1-8) | Avg. (2-7) | Luxmeters | | | | | | | | Avg. (1-8) | Avg. (2-7) |
| | 1 | 2 | 3 | 4 | 5 | 6 | 7 | 8 | | | 1 | 2 | 3 | 4 | 5 | 6 | 7 | 8 | | |
| Relux | 167 | 96 | 27 | 26 | 43 | 10 | 96 | 39 | 63 (21.4%) | 50 (20.7%) | 206 | 97 | 27 | 80 | 97 | 49 | 73 | 44 | 84 (22.2%) | 71 (20.4%) |
| Ours with CAD (no LDC LSC) | 188 | 150 | 33 | 45 | 43 | 34 | 91 | 65 | 81 (27.5%) | 66 (27.3%) | 207 | 114 | 99 | 148 | 105 | 117 | 93 | 81 | 120 (31.8%) | 112 (32.2%) |
| Ours with CAD (LDC) | 199 | 152 | 29 | 41 | 40 | 33 | 95 | 57 | 81 (27.5%) | 65 (26.9%) | 213 | 117 | 82 | 125 | 97 | 97 | 86 | 63 | 110 (29.1%) | 100 (28.8%) |
| Ours with CAD (LSC) | 73 | 45 | 24 | 32 | 40 | 34 | 46 | 52 | 43 (14.6%) | 37 (15.3%) | 69 | 80 | 98 | 136 | 70 | 84 | 56 | 62 | 82 (21.7%) | 87 (25.0%) |
| Ours with CAD (LDC LSC) | 69 | 24 | 22 | 38 | 28 | 28 | 38 | 41 | 36 (12.2%) | 30 (12.4%) | 70 | 57 | 76 | 106 | 75 | 69 | 55 | 53 | 70 (18.5%) | 73 (21.0%) |
| Ours with CAD Camera visible (LDC LSC) | - | 64 | 28 | 20 | 17 | 22 | 52 | - | - | 34 (14.1%) | - | 54 | 36 | 59 | 101 | 69 | 54 | - | - | 62 (17.8%) |
| Ours RGB2Lux (LDC LSC) | - | 53 | 41 | 67 | 68 | 40 | 98 | - | - | 61 (25.3%) | - | 98 | 90 | 85 | 136 | 108 | 77 | - | - | 99 (28.5%) |

Table 1: Illumination estimation errors by the considered approaches, applied to both rooms. Values for individual luxmeters, cols 1-8, correspond to the average lux values estimated over the results of the 31 different lighting combinations applied. Avg. (1-8) corresponds to the total average values for all installed luxmeters. By contrast, Avg. (2-7) only considers those luxmeters which are visible from the RGBD camera, *i.e.* within its field-of-view. The percentage values correspond to the lux average percentage error in regards to the ground truth.

ter sensors (x-axis). In each column of the box plots, the 31 gray dots represent the measured error of each of the lighting scenarios. The pink box represents the central 50% of the data, while the upper and lower vertical lines indicate the extension of the remaining error points outside it. The central red line indicates the median error.

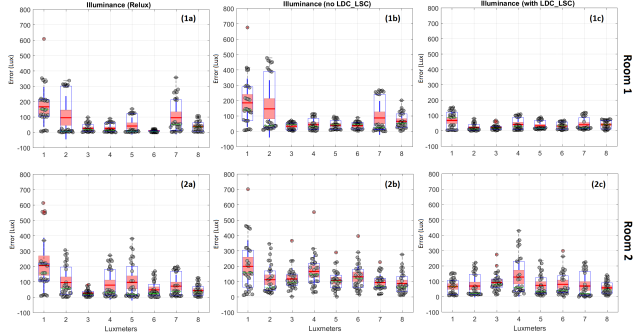


Figure 6. Room 1 & 2 lux boxplot error evaluation using the full CAD information against (a) Relux software, (b) standard radiosity model and (c) radiosity with LDC LSC applied.

In Figure 6, we note a similar performance of Relux (leftmost box plots) and ours without LDC and LSC corrections, for both rooms (top and bottom rows), in line with the findings of Table 1. Interestingly, highest errors occur at luxmeters 1, 2, and 7, which are closely localized under the luminaires and “looking” directly at the light source (check Figure 4 for the geometrical distribution). At these positions, the larger errors are due to a lower illuminance estimation by the radiosity model⁴ as it is also exemplified in Fig. 9.

⁴See the signed plots in the supplementary material.

The rightmost plots in Figure 6 clearly show that the LDC LSC corrections are highly beneficial. The error reduces across all luxmeters and most prominently for those luxmeters 1, 2 and 7, addressing the orthogonally-incident light.

Of particular interest is the case of luxmeter 4 for room 2, whereby the error remains larger. Figure 7 shows the region where the luxmeter is located and this reveals the cause of the issue. The screen monitor shields (occludes) luxmeter 4 from the light of some of the luminaires. Since the simplified CAD model does not include the monitor, the radiosity cannot model the occlusion properly.

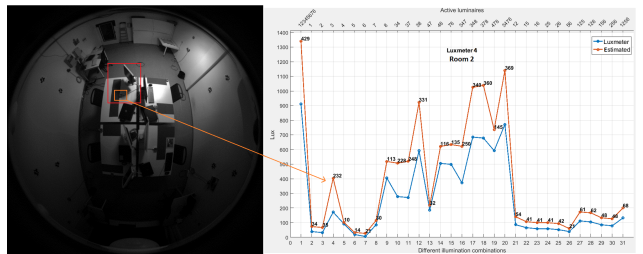


Figure 7. A detailed description of the problem for luxmeter 4 in room 2. There are higher errors due to shadows on the luxmeter sensor and inaccuracy in the 3D CAD model. The graph plot next shows the correlation of the sensor’s measurement and which light activation the error is a result of.

Before we move to the depth based simulations we established another experiment where we simulated a partial part of the CAD model. Here we simulate that the only CAD information available is the one actually visible by the camera. Such information might be available for instance to a

depth camera observing the scene. In such case almost 60% of the room is not visible so providing a real challenge for our light estimation system. Figure 8 shows the results for our radiosity with LDC_LSC model since i) it is the best performing against standard radiosity, ii) Relux software does not work with open surface (while we do).

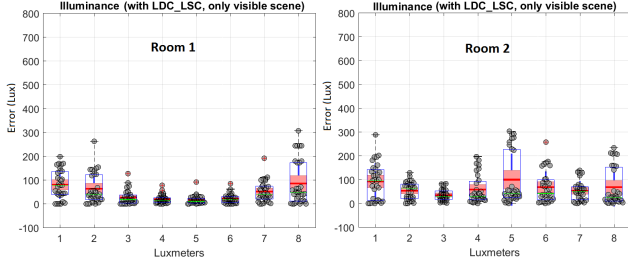


Figure 8. Room 1 & 2 Lux boxplot error evaluation using only the visible CAD information on the radiosity with LDC_LSC.

Note the increment in the error for luxmeters 1, 2 and 8, especially in room 1, in comparison to Figure 6 (1c), which are closer to the walls. Since part of the walls are not visible (because they are not included in the camera field of view) the form factors fail to grasp the light contribution of the wall reflections (see Figure 8).

4.4. Light measurements from RGBD data

Here we evaluate the performance of our proposed RGBD2lux. We use just the RGBD image and apply the correcting LDC and LSC curves to the radiosity model.

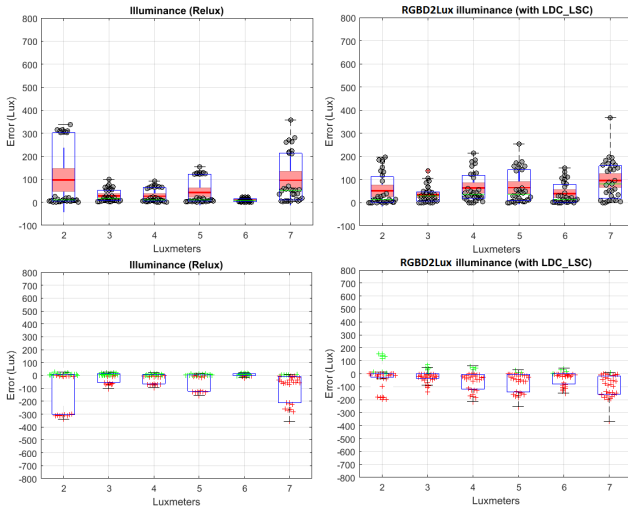


Figure 9. The figure shows the comparison between the Relux simulation with CAD model (left) and our RGBD2lux approach (right) for room 1. Even if our method do not use the CAD model it achieves better or equivalent performance in some scenarios. Plots in the second row specify the type of the error, i.e. due to lower (red marker) or over (green marker) estimation.

The box plots in Figure 9 show that RGBD2Lux achieves better or equivalent performance than the Relux simulation in some of the 31 lighting scenarios tested. Note that in the estimated results with the depth input the error is mainly due to lower estimation of the illumination levels within the room as a cause of the missing geometry. However, considering also the incomplete geometry, this experiment shows that even with partial geometry information given by a depth sensor our system can match or even overcome the CAD-based (with full geometry given) state of the art in challenging scenarios (similar results are obtained for room 2 and included in the supplemental material). The computational time for our modelling is approx. 3-5 minutes (Matlab) while Relux requires approx. 15-20 minutes respectively.

5. Conclusions

The proposed RGBD2lux method can be a viable option for estimating light intensity in a real environments. Interestingly enough we show that it is possible to challenge or even surpass current state-of-the-art light planning and modeling simulation software where the complete CAD model geometry is a necessary requirement, by using a partial geometry obtained from a camera sensor. Moreover, we show that the RGBD sensor, even if providing noisy information, can be a more realistic expression of the 3D structure of the current scene. Even the most accurate CAD model might not be aware about changes on the room structure that happens after the original planning.

This study provides a new direction for the research in lighting and for the lighting industry based on imaging and visual computing. On one side, we show that continuous and reliable camera-aided measurements of light on real environments is now viable, possibly enabling the study of how light dynamics do influence human health, habits, social activities, to quote a few. The proposed lighting model can surely be improved and further experiments can be conducted, taking into account other material (e.g. specular components, caustics, etc.) and scene (e.g. dynamic scenes with people) properties or even go for a fully automatic solution where the positioning of the light sources will also be estimated. On the other side, lighting companies may design modules specifically suited for a fast and reliable light measurement. If attached to dimmable light sources, these modules may represent a major improvement for smart lighting, where light level is continuously updated to ensure maximum comfort and well-being.

Acknowledgments: The authors would like to thank Luc Masset for his insightful feedback. This project has received funding from the European Union's Horizon 2020 research and innovation programme under the Marie Skłodowska-Curie Grant Agreement No. 676455.

References

- [1] Dial gmbh: Dialux. <https://www.dial.de/en/dialux/>. Accessed: 2017-11-16.
- [2] Lighting analysts, inc. <http://www.agi32.com>. Accessed: 2017-11-16.
- [3] Relux informatik ag: Reluxdesktop. <https://relux.com/en/>. Accessed: 2017-11-16.
- [4] Vrvs research center: Hilite. <http://www.vrvis.at/projects/hilite>. Accessed: 2018-05-23.
- [5] Ward g.: Radiance renderer. <http://radsite.lbl.gov/radiance>. Accessed: 2017-11-16.
- [6] R. Basri, D. Jacobs, and I. Kemelmacher. Photometric stereo with general, unknown lighting. *International Journal of Computer Vision*, 72(3):239–257, 2007.
- [7] B. Beckers and P. Beckers. Fast and accurate view factor generation. *FICUP, An International Conference on Urban Physics*, 09 2016.
- [8] H. Cai. Luminance gradient for evaluating lighting. *Lighting Research & Technology*, 48(2):155–175, 2016.
- [9] M. Chandraker, J. Bai, T.-T. Ng, and R. Ramamoorthi. On the duality of forward and inverse light transport. *IEEE Trans. Pattern Anal. Mach. Intell.*, 33(10):2122–2128, Oct. 2011.
- [10] T. L. Choo and O. H. See. *Illuminance Calibration of A Digital Camera based on Image Colour*. The 3rd National Graduate Conference (NatGrad2015), Universiti Tenaga Nasional, Putrajaya Campus, 2015.
- [11] M. F. Cohen and D. P. Greenberg. The hemi-cube: A radiosity solution for complex environments. *SIGGRAPH Comput. Graph.*, 19(3):31–40, July 1985.
- [12] M. F. Cohen, J. Wallace, and P. Hanrahan. *Radiosity and Realistic Image Synthesis*. Academic Press Professional, Inc., San Diego, CA, USA, 1993.
- [13] R. L. Cook, T. Porter, and L. Carpenter. Distributed ray tracing. *SIGGRAPH Comput. Graph.*, 18(3):137–145, Jan. 1984.
- [14] C. Cuttle. Towards the third stage of the lighting profession. *Lighting Research & Technology*, 42(1):73–93, 2010.
- [15] C. M. Goral, K. E. Torrance, D. P. Greenberg, and B. Battaile. Modeling the interaction of light between diffuse surfaces. *SIGGRAPH Comput. Graph.*, 18(3):213–222, Jan. 1984.
- [16] T. Hachisuka, S. Ogaki, and H. W. Jensen. Progressive photon mapping. *ACM Trans. Graph.*, 27(5):130:1–130:8, Dec. 2008.
- [17] P. D. Hiscocks and P. Eng. Measuring luminance with a digital camera. Technical report, Syscomp Electronic Design Limited, 2014.
- [18] J. F. Hughes and J. D. Foley. *Computer graphics: principles and practice*. Pearson Education, 2014.
- [19] H. W. Jensen. Global illumination using photon maps. In *Proceedings of the Eurographics Workshop on Rendering Techniques '96*, pages 21–30, London, UK, UK, 1996. Springer-Verlag.
- [20] J. T. Kajiya. The rendering equation. *SIGGRAPH Comput. Graph.*, 20(4):143–150, Aug. 1986.
- [21] M. Kazhdan and H. Hoppe. Screened poisson surface reconstruction. *ACM Transactions on Graphics (ToG)*, 32(3):29, 2013.
- [22] A. Keller. Instant radiosity. In *Proceedings of the 24th Annual Conference on Computer Graphics and Interactive Techniques, SIGGRAPH '97*, pages 49–56, New York, NY, USA, 1997. ACM Press/Addison-Wesley Publishing Co.
- [23] J. Krivanek, A. Keller, I. Georgiev, A. S. Kaplanyan, M. Fajardo, M. Meyer, J.-D. Nahmias, O. Karlik, and J. Canada. Recent advances in light transport simulation: Some theory and a lot of practice. In *ACM SIGGRAPH 2014 Courses*, SIGGRAPH '14, pages 17:1–17:6, NY, USA, 2014. ACM.
- [24] K. Krsl, C. Luksch, M. Schwärzler, and M. Wimmer. LiteMaker: Interactive Luminaire Development using Progressive Photon Tracing and Multi-Resolution Upsampling. In M. Hullin, R. Klein, T. Schultz, and A. Yao, editors, *Vision, Modeling & Visualization*. The Eurographics Association, 2017.
- [25] J. Lambert and E. Anding. *Photometrie: Photometria, sive De mensura et gradibus luminis, colorum et umbrae (1760)*. Ostwalds Klassiker der exakten Wissenschaften. W. Engelmann, 1870.
- [26] W.-C. Lin, T.-S. Huang, T.-C. Ho, Y.-T. Chen, and J.-H. Chuang. Interactive lighting design with hierarchical light representation. In *Proceedings of the Eurographics Symposium on Rendering, EGSR '13*, pages 133–142, Aire-la-Ville, Switzerland, Switzerland, 2013. Eurographics Association.
- [27] C. Luksch, R. F. Tobler, R. Habel, M. Schwärzler, and M. Wimmer. Fast light-map computation with virtual polygon lights. In *Proceedings of the ACM SIGGRAPH Symposium on Interactive 3D Graphics and Games, I3D '13*, pages 87–94, New York, NY, USA, 2013. ACM.
- [28] C. Luksch, R. F. Tobler, T. Mühlbacher, M. Schwärzler, and M. Wimmer. Real-time rendering of glossy materials with regular sampling. *Vis. Comput.*, 30(6-8):717–727, June 2014.
- [29] H. Maitre. From photon to pixel: The digital camera handbook, 2015.
- [30] T. Malley. A shading method for computer generated images. *Master's thesis, Dept. of Computer Science, University of Utah*, 1988.
- [31] S. Marschner and P. Shirley. *Fundamentals of computer graphics*. CRC Press, 2015.
- [32] S. R. Marschner and D. P. Greenberg. Inverse lighting for photography. In *Color and Imaging Conference*, volume 1997, pages 262–265. Society for Imaging Science and Technology, 1997.
- [33] L. Masset, O. Bröls, and G. Kerschen. Partition of the circle in cells of equal area and shape. Technical report, Structural Dynamics Research Group, Aerospace and Mechanical Engineering Department, University of Liege, 'Institut de Mecanique et Genie Civil (B52/3), 2011.
- [34] R. Ramamoorthi and P. Hanrahan. A signal-processing framework for inverse rendering. In *Proceedings of the 28th annual conference on Computer graphics and interactive techniques*, pages 117–128. ACM, 2001.

- [35] M. Schwarz and P. Wonka. Procedural design of exterior lighting for buildings with complex constraints. *ACM Trans. Graph.*, 33(5):166:1–166:16, Sept. 2014.
- [36] J. Sorger, T. Ortner, C. Luksch, M. Schwärzler, E. Gröller, and H. Piringer. Litevis: integrated visualization for simulation-based decision support in lighting design. *IEEE Transactions on Visualization and Computer Graphics*, 22(1):290–299, 2016.
- [37] T. Tsesmelis, I. Hasan, M. Cristani, A. Del Bue, and F. Galasso. LIT: A system and benchmark for light understanding. In *2017 IEEE International Conference on Computer Vision Workshops, ICCV Workshops 2017, Venice, Italy, October 22-29, 2017*, pages 2953–2960, 2017.
- [38] J. Van Leersum. A method for determining a consistent set of radiation view factors from a set generated by a nonexact method. *International journal of heat and fluid flow*, 10(1):83–85, 1989.
- [39] E. Veach and L. J. Guibas. Optimally combining sampling techniques for monte carlo rendering. In *Proceedings of the 22nd annual conference on Computer graphics and interactive techniques*, pages 419–428. ACM, 1995.